European Journal of Oral Sciences

Eur J Oral Sci 2015; 123: 228–234
DOI: 10.1111/eos.12197

European Journal of Oral Sciences

Morphological analyses and a novel *de novo DLX3* mutation associated with tricho–dento–osseous syndrome in a Chinese family

Yue Li[1,*], Dong Han[1,*], Hao Zhang[1,*], Haochen Liu[1], Singwai Wong[1], Na Zhao[1], Lixin Qiu[2], Hailan Feng[1]

[1]Department of Prosthodontics, Peking University School and Hospital of Stomatology; [2]The 4th Dental Division, Peking University School and Hospital of Stomatology, Beijing, China

*These authors contributed equally to this work.

Li Y, Han D, Zhang H, Liu H, Wong S, Zhao N, Qiu L, Feng H. Morphological analyses and a novel de novo DLX3 *mutation associated with tricho–dento–osseous syndrome in a Chinese family.*
Eur J Oral Sci 2015; 123: 228–234. © 2015 Eur J Oral Sci

Tricho–dento–osseous (TDO) syndrome, an autosomal-dominant disorder, affects the morphological appearance of the tooth enamel, hair, and bone. Previous studies have confirmed that mutations in the *DLX3* gene are responsible for TDO. In this study, we describe a Chinese patient with the typical traits of TDO – kinky hair, enamel hypoplasia, skull and jaw bones thickening, and sclerosis. Unfortunately, as a result of excessive attrition, we were unable to assess taurodontism. Examination of the tooth ground section showed a thin layer of enamel with no rods on the patient's tooth and abnormalities in Tomes' granular layer and the dentinal tubules. Scanning electron microscopy and energy-dispersive X-ray spectroscopy of the tooth enamel showed significant differences between the patient and the control individuals. A hair sample from the patient observed under a laser-scanning microscope showed longitudinal grooves in the hair shaft. Dual-energy X-ray absorptiometry measurement showed that the bone mineral density values of the patient's bones was much higher than normal. Finally, genetic analysis revealed a novel *de novo* missense mutation c.533A>G (p.Q178R) in the conserved homeodomain of the *DLX3* gene. This *DLX3* mutation is the sixth causative mutation for TDO to be identified so far.

Hailan Feng, Department of Prosthodontics, Peking University School and Hospital of Stomatology, 22 Zhongguancun Nandajie, Haidian District, Beijing 100081, China

E-mail: kqfenghl@bjmu.edu.cn

Key words: *DLX3*; enamel hypoplasia; jaw bones thickening; kinky hair; tricho–dento–osseous syndrome

Accepted for publication May 2015

Tricho–dento–osseous syndrome (TDO; OMIM 190320) is a rare genetic disorder with an autosomal-dominant mode of inheritance; it mainly affects the hair, teeth, and bones. Tricho–dento–osseous syndrome is considered as a form of ectodermal dysplasia with an unknown incidence rate. Its main clinical manifestations are kinky hair at birth, severely hypoplastic enamel, taurodontism, and sclerosis of the bones. Other minor manifestations reported are skin lesions (1), frontal bossing (2, 3), and splitting of the superficial layers of the nails (4, 5). In 1993, Seow (3) proposed that a positive identification of TDO should include following main criteria: generalized enamel defects that show hypomaturation or hypocalcification along with enamel hypoplasia; severe taurodontism of the teeth involving the mandibular first permanent molars; an autosomal-dominant mode of inheritance; and at least one other feature (i.e. nail defects; bone sclerosis; and curly, kinky, or wavy hair at a young age, which may straighten out later). However, because of the clinical variations in the presentation of TDO, the diagnostic criteria remain unclear.

Lichtenstein *et al.* (2) first described TDO as a distinct condition in an Irish–American kindred (of 169 members through six generations), from Washington County, VA, USA, in 1971. In 1997, Price *et al.* (6) identified a four-base-pair deletion in the distal-less homeobox 3 (*DLX3*) gene in TDO-affected individuals, which caused a frameshift mutation and the formation of a truncated protein; however, the homeodomain was intact. This was the first report of a *DLX3* mutation associated with TDO. To date, five different mutations in the *DLX3* gene have been identified in TDO patients of different races (1, 6–9), but no such mutations have been identified in the Chinese population.

DLX3, which is located on chromosome 17q21, codes for a transcription factor that plays an indispensible role in placenta formation and embryonic development. Loss of *Dlx3* in *Dlx3*-null mice is embryonic lethal (10). *Dlx3* is expressed in structures involving epithelial–mesenchymal interaction, such as the teeth, hair follicles, and skin (11) and has been shown to play a crucial role in tooth development (12), hair differentiation and regeneration (13), and in osteoblastic differentiation

and bone formation (14, 15). Misexpression of *Dlx3* results in the transformation of basal cells into more highly differentiated keratinocytes and reduced stratification of the epidermis (16). Thus, defects in the expression of this protein are clearly associated with the clinical features of TDO, and it is therefore important to examine patients who show symptoms of TDO for *DLX3* mutations.

In this study, we describe a Chinese patient with many of the features associated with TDO. Morphological analyses revealed thickened and increased density of skull and jaw bones, the existence of a thin layer of non-prismatic tooth enamel, and abnormal longitudinal grooves in the hair shaft. In addition, DNA sequencing identified a novel *de novo* mutation in the *DLX3* gene in this patient. This is the first time that a *DLX3* mutation has been reported in the Chinese population.

Material and methods

Participants

A 27-yr-old female patient with a full mouth of residual roots was referred to the Department of Prosthodontics, Peking University School of Stomatology, for dental treatment. Oral examination of the patient, her parents, and her younger brother was performed by a prosthodontist, who determined the status of the dentition. A panoramic radiograph was taken to observe defects of the teeth and craniofacial bones. The shape and size of the residual teeth were also observed. The patient's general health, including ectodermal features and other syndromic indications, was assessed by clinical examination and interviews. One-hundred volunteers without any hair, tooth, or bone abnormalities were recruited as controls.

Informed consent for DNA analysis and reproduction of the photographs was obtained from all participants. This study was conducted with the approval of the Ethics Committee of Peking University Health Science Center.

Histological examination

Because restoration of all the patient's 32 teeth with obvious periapical abscesses would not have been possible, they were extracted and fixed in 10% neutral-buffered formalin. Five teeth of each tooth type (incisor, canine, premolar, and molar), with healthy enamel and no caries or fracture, were selected among the extracted teeth from the Department of Oral and Maxillofacial Surgery, Peking University School of Stomatology, and used as control teeth. For examination of methacrylate-embedded tooth ground sections, after rinsing and removal of the superficial impurities, two molars (upper left third and lower right second) and one premolar (upper left second) were embedded in polymerizing methyl methacrylate monomer (9) and axially sectioned along the buccal–lingual plane at a thickness of 100–150 μm, using a low-speed saw microtome (Leitz 1600; Leica Biosystems, Wetzlar, Germany). The tooth sections were polished with a whetstone and cleaned thoroughly with an ultrasonic cleaner (17). After dehydration in an ethanol gradient, the section was immersed in xylene for 1 min. Then, neutron-gum was used to block the section for observation. Finally, the tooth section was observed and photographed using a polarizing microscope (OLYMPUS BX51; Olympus, Tokyo, Japan).

For scanning electron microscopy and energy-dispersive X-ray spectrometry (EDX) analyses, one incisor (upper left central) and one premolar (upper left first) were cut into two parts labiolingually using a chisel to preserve the surface details (18). One-half of the tooth was etched with 30% phosphoric acid for 30 s and the other half was not etched; all sections were rinsed with distilled water and dried in a heating oven at 37°C for 24 h (19). The tooth samples were mounted on metal stubs and coated with gold using the standard evaporation technique (20). Then, the tooth samples were observed using a scanning electron microscope (HITACHI S4800; HITACHI, Tokyo, Japan). Elemental analysis was performed using an energy-dispersive X-ray spectrometer (EMAX; HORIBA, Kyoto, Kyoto-fu, Japan). The amounts of carbon (C), oxygen (O), calcium (Ca), and phosphorus (P) were measured.

Three-dimensional laser-scanning microscopy

Hairs taken from the patient, her parents, and her younger brother were fixed on a slide and observed using a laser microscope (VK-X100/X200; KEYENCE, Osaka, Osaka-fu, Japan). The image was compared with the image of a hair taken from a control.

Dual-energy X-ray absorptiometry

The bone mineral density (BMD) value of the patient's axial and peripheral bones was measured using dual-energy X-ray absorptiometry (DXA) with Hologic Discovery A (Hologic, Boston, MA, USA) and was compared with the average BMD value at the corresponding site of the body of healthy Chinese women of 25–29 yr of age. These average BMD values were available from the study of Wu *et al*. (21).

DNA extraction, detection of mutations, and conservation analysis

Genomic DNA of the patient, her parents, her younger brother, and 100 controls was extracted from peripheral blood lymphocytes using the Biotek DNA minikit (Biotek, Beijing, China). DNA samples of the controls were extracted from buccal epithelial cells using the Chelex-100 (Sigma, St Louis, MO, USA) method.

All three *DLX3* exons, including the exon–intron boundaries, were amplified by PCR using the Go Taq GreenMaster Mix (Promega, Madison, WI, USA). The primer sequences and the PCR conditions for *DLX3* were as described in Kim *et al*. (22). The PCR products were sequenced by Sangon Biotech Company (Beijing, China) using BIGDYE TERMINATOR v3.1 (Applied Biosystems, Foster City, CA, USA) and a 3730 DNA sequencer (Applied Biosystems). The SEQMAN PRO genetic analysis software (DNASTAR, Madison, WI, USA) was used for sequencing analysis. The identified mutation was bioinformatically verified using the SIFT software (http://sift.jcvi.org/www/SIFT_enst_submit.html) and POLYPHEN-2 modeling software (http://genetics.bwh.harvard.edu/pph2/). The conservation of residues in sequences was investigated in order to predict the influence of the mutation on *DLX3*. The sequences of orthologs of human DLX3 protein were

retrieved from the ENSEMBL database (http://asia.ensembl.org/Homo_sapiens/Gene/Compara_Ortholog?db=core;g=ENSG00000064195;r=17:49990005-49995224); these sequences were used to perform sequence alignment with CLUSTALX 2.1 and JALVIEW.

Results

Clinical characteristics

The patient's height was 164 cm, showing a normal stature compared with the general population of Chinese female adults of the same age. All her permanent teeth had erupted, including the four-third molars. Hypoplastic enamel with a yellow/brown discoloration was observed in the dentition of the patient (Fig. 1A). The teeth showed severe attrition, which resulted in considerably short clinical crowns or residual roots; furthermore, the fistula could also be seen in the gingiva (Fig. 1A). A panoramic radiograph revealed that most of her teeth had been endodontically treated, and some periapical lesions can be observed. Although the furcation of the lower left second molar was apically displaced, it was not possible to determine the crown:root ratio as a result of attrition and loss of occlusal pattern. Besides, no pulp chamber enlargement was detected. These findings were not definitely indicative of taurodontism. Furthermore, the trabeculae of the mandible were significantly obscure (Fig. 1B). Unlike the normal black, straight hair found in Chinese people, the patient's hair was sparse, of light color, and kinky, as it had been since birth (Fig. 1C). Frontal

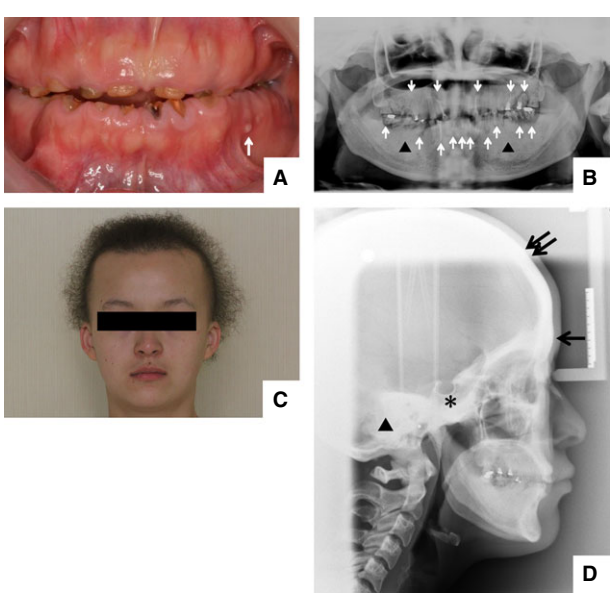

Fig. 1. Clinical characteristics of the patient with tricho–dento–osseous (TDO) syndrome. (A) All teeth were small, yellow/brown colored, and lacked enamel. The white arrow indicates the fistula in the gingiva. (B) Panoramic radiograph showing no obvious taurodontism. White arrows indicate the endodontically treated teeth. Black triangles indicate the abnormal trabeculae of the mandible. (C) Frontal view: curly kinky hair and frontal bossing can be seen. (D) Lateral cephalometric radiograph showing increased thickness and density of the skull bones and jaw bones, especially the skull base region. The black arrow indicates the absence of the frontal sinus; the double black arrow indicates obliteration of the diploë; the black asterisk indicates the thickened and sclerosed skull base region; and the black triangle indicates obliteration of the mastoid air cells.

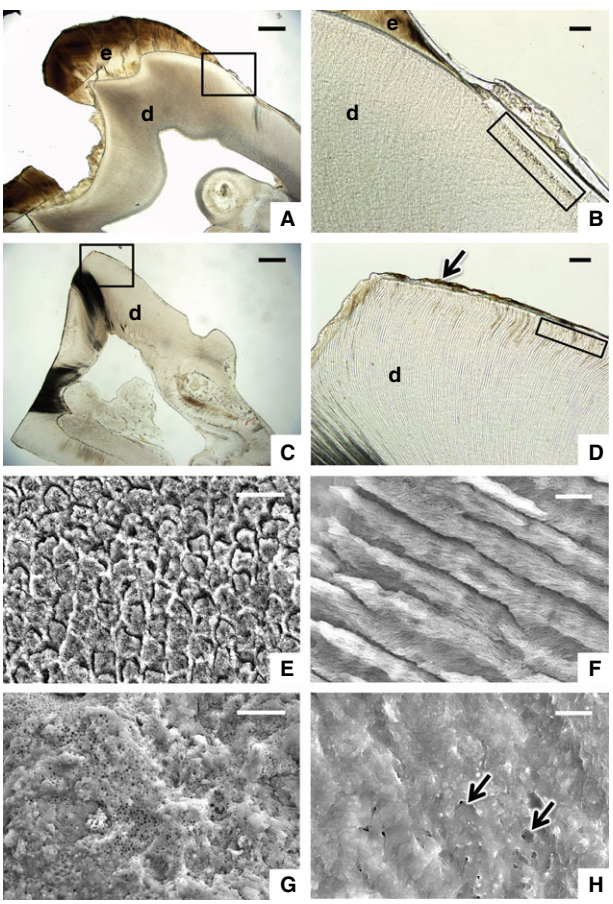

Fig. 2. Histological appearance of the ground section and findings of scanning electron microscopy and energy dispersive X-ray spectrometry (EDX) analyses. (A–D) Microscopic appearance of the upper-left third molar from the control teeth (A, B) and the patient (C, D). (A) The enamel and dentin are evident. (B) Higher-magnification view of the boxed area in (A). The enamel rods are evident. The box indicates regular arrangement of Tomes' granular layer and the end of the dentinal tubules. (C) Hardly any enamel is visible. (D) Higher-magnification view of the boxed areas in (C). The black arrow indicates a thin layer of enamel without enamel rods. The box indicates the sparseness of Tomes' granular layer and the curved end of the dentinal tubules. (E–H) Scanning electron microscopy images of the upper-left central incisor from the control teeth (E, F) and the patient (G, H). (E) Normal enamel with well-organized and distinct enamel rods on the labial surface. (F) Regular arrangement of enamel rods of the cut surface. (G) Loose and rough enamel of the labial surface with a porous structure. (H) Amorphous cut surface showing lack of visible enamel rods. The black arrow indicates the porous area. d, dentin; e, enamel. Scale bars: 1 mm in A and C; 100 μm in B and D; 10 μm in E and G; 5 μm in F and H.

bossing was also observed (Fig. 1C). A lateral cephalometric radiograph showed the increased thickness and density of the skull bones and jaw bones, especially the skull base region, obliteration of the diploë, and absence of the frontal sinus and the mastoid air cells (Fig. 1D). No engagement of the nail defect, skin lesions, or other abnormalities was observed. No other member of the patient's family showed similar tooth, hair, or bone abnormalities. Her parents denied consanguineous marriage or any remarkable events during pregnancy.

Histological findings for the teeth

Macroscopic examination showed that all the teeth were small, with short clinical crowns and partial loss of enamel as a result of severe attrition. Examination of the methacrylate-embedded ground sections showed no obvious enamel near the enamel–cementum junction (CEJ) (Fig. 2C), compared with the control teeth (Fig. 2A). However, under a higher-magnification view, a fairly thin layer of amorphous enamel was detected near the CEJ (Fig. 2D). Enamel rods were invisible compared with the control teeth (Fig. 2B). The cementum and Tomes' granular layer could be identified, but they were relatively sparse in some areas of the root compared with the dentition of the control teeth. The dentinal tubules adjacent to the CEJ were more curved (Fig. 2D) than those of the control teeth (Fig. 2B).

Using scanning electron microscopy, we found that the tooth enamel in the control teeth was smooth and that the labial and cut surfaces showed a well-organized distinct rod appearance (Fig. 2E,F). However, the patient's tooth enamel showed a highly rough, porous and non-prismatic labial surface, and the crystals were difficult to identify (Fig. 2G). Furthermore, the cut surface of the patient's tooth was characterized by a layer that lacked obvious structure; the rod boundaries and crystals of the enamel were severely blurred and indistinguishable; and the structure appeared porous (Fig. 2H). Elemental analysis of the patient's teeth by EDX revealed a dramatic increase in the C:O ratio and a significant reduction of weight and atomic percentage of Ca, compared with that of the control teeth, respectively (Table 1); however, P was not detected in the irregular rod structures of the patient's incisor (Table 1).

Table 1

Energy-dispersive X-ray spectrometry (EDX) spectra of the cut surface of the upper left central incisor from the control teeth and the patient

	Weight percentage (%)		Atomic percentage (%)	
Element	Controls	Patient	Controls	Patient
C	8.24 ± 0.21	62.84	15.37 ± 0.55	70.11
O	36.93 ± 0.70	34.69	51.77 ± 0.97	29.06
P	17.67 ± 0.81	N/A	12.79 ± 0.58	N/A
Ca	37.16 ± 0.88	2.47	20.83 ± 0.49	0.83

C, carbon; Ca, calcium; N/A, not available; O, oxygen; P, phosphorus. Values of the control teeth are given as mean ± SD.

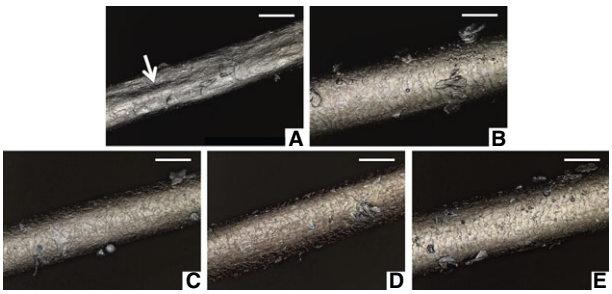

Fig. 3. Laser-scanning microscopy observation of hair. (A) Hair from the patient: the white arrows indicate the longitudinal grooves and scarce scales. (B) Hair from a control. (C) Hair from the patient's father. (D) Hair from the patient's mother. (E) Hair from the patient's younger brother. Scale bars: 50 μm.

Table 2

Patient's bone mineral density (BMD) values in different regions of the body

Body region	BMD (g cm^{-2})
Left arm	0.823
Right arm	0.891
Left ribs	0.909
Right ribs	0.789
Thoracic spine	1.207
Lumbar spine	1.602
Pelvis	2.218
Left leg	1.428
Right leg	1.454
Head	3.919

Three-dimensional laser-scanning microscopy of the hair

Longitudinal grooves along the hair shaft could be observed, and scales through the hair shaft appeared amorphous and scarce under the laser microscope (Fig. 3A). These observations were different from those for the controls, which showed dense and well-organized scales and no longitudinal grooves (Fig. 3B). The hairs of the patient's parents (Fig. 3C,D) and her younger brother (Fig. 3E) showed a normal shaft compared with that of the controls.

DXA Findings

The BMD value of the patient's right hip was 1.581 g cm^{-2} (Supporting Fig. S1A), which was much higher than the average BMD value (0.854 ± 0.092 g cm^{-2}) of Chinese healthy women at the same body region (21). The BMD value of the patient's lumbar spine, L1–L4, was 1.602 g cm^{-2} (Fig. S1B), which was much higher than the average BMD value (0.948 ± 0.090 g cm^{-2}) of the Chinese healthy women at the same body region (21). Further-

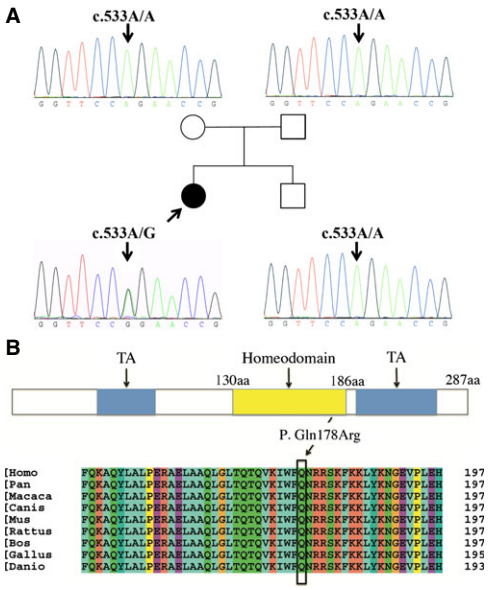

Fig. 4. Sequence analysis of the distal-less homeobox 3 (*DLX3*) gene and structure and conservation analysis of the *DLX3* mutation. (A) The *DLX3* mutation c.533A>G was detected in the patient, but was not found in her father, mother, or younger brother. The mutation is marked with an arrow at its corresponding position in the gene sequence. (B) Conservation analysis of nine different vertebrate species indicates that Gln178 in the *DLX3* protein is highly conserved. aa, amino acid; TA, transcription activation domain.

more, the BMD value of her head (3.919 g cm^{-2}) was higher than the rest of the parts of the patient's body (Table 2; Fig. S1C).

Detection of the *DLX3* mutation and conservation analysis

The nucleotide sequence showed an A to G transition at nucleotide 533 (c.533A>G) of the coding region within exon 3 of *DLX3* (Fig. 4A), which results in the substitution of glutamine (Q), at nucleotide position 178, with arginine (R) (p.Q178R). This substitution was not detected in the patient's family members (Fig. 4A) and was not reported previously (Table 3). This novel *de novo DLX3* mutation was not found in the controls.

Gln178 is located in the homeodomain of the DLX3 protein (Fig. 4B). Multiple-species amino-acid sequence alignment analysis of the DLX3 protein showed that Gln178 was highly conserved during evolution (Fig. 4B). We performed bioinformatic analysis and found that the Q178R mutation in DLX3 was predicted to be probably damaging (Fig. S2).

Discussion

In this study, we performed morphological and genetic analyses in a Chinese patient with TDO. The patient was phenotypically distinguished by kinky hair, enamel hypoplasia, and increased thickness and sclerosis of the skull bones. These characteristics are mostly in accordance with those reported previously (1–3, 7–9). Gorlin *et al.* (24) reported that TDO may occur as two forms, TDO-I and TDO-II. According to differences in clinical features between TDO-I and TDO-II, our patient is prone to be classified as TDO-II (Supporting Table S1). Furthermore, we found that the density of the jaw bones was increased and the trabeculae of the mandible were obscure, which suggests that the mandibular bone might be sclerosed. It is worth noting that these morphological changes of the jaw bones in patients with TDO have not been described previously. Additionally, the patient had dramatically attrited teeth. We found a thin layer of enamel near the CEJ of the proximal surface of the ground sections, which was in accordance with the findings of Nieminen *et al.* (9). Moreover, we found that the enamel surface was rough, porous, and lacked the normal rod appearance, which was in accordance with the clinical phenotype of enamel hypoplasia. Energy-dispersive X-ray spectrometry provided evidence of enamel hypomineralization (25), based on the considerably high C:O ratio, low weight and atomic percentage of Ca, and absence of P. Tomes' granular layer was partially sparsely arranged and the ends of the dentinal tubules were more curved in the ground section, which suggests that dentinal development might also be compromised in this patient. No study has previously reported abnormalities in the Tomes' granular layer or in EDX results on TDO cases. Enamel hypoplasia and hypomineralization, combined with dentinal defects, may be the main cause of severe tooth attrition and periapical lesions in our patient. Seow (26) pointed out that taurodontism of the mandibular first permanent molars may be a key

Table 3

*Mutations identified in the distal-less homeobox 3 (*DLX3*) gene*

Exon	cDNA	Amino acid	Mutation type	Diagnosis	Reference
3	561–562delCT	p.Tyr188GlnfsX13	Frameshift	AIHHT	23
3	561–562delCT	p.Tyr188GlnfsX13	Frameshift	TDO	7, 8
3	571–574delGGGG	p.Gly191ArgfsX66	Frameshift	TDO	6
2	398G>C	p.Arg133Pro	Missense	TDO	9
3	524T>C	p.Ile175Ser	Missense	TDO	1
3	533A>G	p.Gln178Arg	Missense	TDO	This study
3	545C>T	p.Ser182Phe	Missense	TDO	9

AIHHT, amelogenesis imperfecta hypoplastic-hypomaturation with taurodontism; TDO, tricho–dento–osseous syndrome.

feature for distinguishing between TDO and amelogenesis imperfecta and also helpful in diagnosing TDO. However, in the study of Lee *et al*. (7), there was no definitive evidence of taurodontic molars; the only change observed in the proband was the extension of the pulp chamber in the maxillary central incisors. In our study, because it was difficult to determine the correct crown:root ratio, we failed to confirm whether taurodontism was present in the patient, based on the criteria proposed by Seow (26). We hypothesize that over-attrition and serious periapical lesions may have led to failure to obtain the correct crown:root ratio or that proliferation of the secondary dentin masked the taurodontism in this patient.

Most of the skull bones were observed in previous studies on patients with TDO; however, the thickness and density of the skull bones among such patients showed wide variation (2, 7–9). In our patient, radiographic evaluation revealed that the thickness and density of her skull bones were obviously increased, and that the diploë, frontal sinus, and mastoid air cells were obliterated. Using DXA, the technique most commonly used for BMD measurement, Wu *et al*. (21) found that the BMD values of healthy Chinese women in the age range of 25–29 yr was 0.854 ± 0.092 g cm^{-2} at total hip and 0.948 ± 0.090 g cm^{-2} at lumbar spine. By comparison, our patient showed a significant increase of BMD values at these two regions, 1.581 g cm^{-2} at the right hip and 1.602 g cm^{-2} at the lumbar spine. Haldeman *et al*. (27) and Wright *et al*. (8) found similar bone changes in their studies. However, no evaluation of head BMD has been reported. In our study, the BMD value of the patient's head was much higher than that of other parts of her body because cranial neural crest cells and cranial paraxial mesoderm cells give rise to osteoblasts and form the craniofacial bones that compose the skull (28, 29), whereas in the trunk and limb regions, osteoblasts are derived from trunk paraxial mesoderm and lateral plate mesoderm (30, 31). The different cell origins may explain the different finding of BMD values on the patient's head and other parts of her body, suggesting that the dosage requirement of DLX signals and the regulatory mechanism of craniofacial osteoblast differentiation may differ from that of trunk or limb.

Laser-scanning microscopy examination of the patient's hair showed abnormal and scarce scales and longitudinal grooves in the hair shaft. This is similar to the findings of other studies, in which scanning electron microscopy analysis has shown the presence of longitudinal grooves in the hair shaft in some patients (1, 32). However, our patient had kinky and light-colored hair, which is extremely unusual in Asian people.

By DNA sequencing, we identified a novel *de novo* *DLX3* missense mutation (c.533A>G) in the patient. Our study is the first to present a *DLX3* mutation in the Chinese population. The mutation leads to a Gln178Arg substitution (p.Q178R) in the homeodomain of DLX3. This novel missense mutation is the sixth causative mutation site detected and the fifth detected within the homeodomain of DLX3. Conservation analysis of nine different vertebrate species indicated that Gln178 was highly conserved, indicating that the mutation might interfere with the function of DLX3. Bioinformatic analysis further suggested that the Q178R mutation probably damages the function of DLX3. However, because the correlation between the genotype and the phenotype have never been analyzed, the definite mechanism of action of DLX3 in TDO remains to be further explored, and functional studies need to be performed to shed light on the pathogenesis of this condition.

Acknowledgements – This study was supported by grants from the National Natural Science Foundation of China (no. 81070814 and no. 81271121) and the Beijing Natural Science Foundation (no. 7092113). We thank all the subjects participating in the research. We thank Prof. Yan Gao (Department of Oral Pathology, Peking University School and Hospital of Stomatology) for his advice on tooth ground section preparation and the histological analysis.

Conflicts of interest – All of the authors declare that there are no conflicts of interest.

References

1. Mayer DE, Baal C, Litschauer Poursadrollah M, Hemmer W, Jarisch R. Uncombable hair and atopic dermatitis in a case of tricho–dento–osseous syndrome. *J Dtsch Dermatol Ges* 2010; **8**: 102–103.
2. Lichtenstein J, Warson R, Jorgenson R, Dorst JP, McKusick VA. The tricho–dento–osseous (TDO) syndrome. *Am J Hum Genet* 1972; **24**: 569–582.
3. Seow WK. Trichodentoosseous (TDO) syndrome: case report and literature review. *Pediatr Dent* 1993a; **15**: 355–361.
4. Robinson GC, Miller JR. Hereditary enamel hypoplasia: its association with characteristic hair structure. *Pediatrics* 1966; **37**: 498–502.
5. Quattromani F, Shapiro SD, Young RS, Jorgenson RJ, Parker JW, Blumhardt R, Reece RR. Clinical heterogeneity in the tricho–dento–osseous syndrome. *Hum Genet* 1983; **64**: 116–121.
6. Price JA, Bowden DW, Wright JT, Pettenati MJ, Hart TC. Identification of a mutation in DLX3 associated with tricho–dento–osseous (TDO) syndrome. *Hum Mol Genet* 1998; **7**: 563–569.
7. Lee SK, Lee ZH, Lee SJ, Ahn BD, Kim YJ, Lee SH, Kim JW. DLX3 mutation in a new family and its phenotypic variations. *J Dent Res* 2008; **87**: 354–357.
8. Wright JT, Hong SP, Simmons D, Daly B, Uebelhart D, Luder HU. DLX3 c.561_562delCT mutation causes attenuated phenotype of tricho–dento–osseous syndrome. *Am J Med Genet A* 2008; **146**: 343–349.
9. Nieminen P, Lukinmaa PL, Alapulli H, Methuen M, Suojarvi T, Kivirikko S, Peltola J, Asikainen M, Alaluusua S. DLX3 homeodomain mutations cause tricho–dento–osseous syndrome with novel phenotypes. *Cells Tissues Organs* 2011; **194**: 49–59.
10. Morasso MI, Grinberg A, Robinson G, Sargent TD, Mahon KA. Placental failure in mice lacking the homeobox gene Dlx3. *Proc Natl Acad Sci USA* 1999; **96**: 162–167.
11. Morasso MI, Mahon KA, Sargent TD. A Xenopus Distal-less gene in transgenic mice: conserved regulation in distal limb epidermis and other sites of epithelial-mesenchymal interaction. *Proc Natl Acad Sci USA* 1995; **92**: 3968–3972.
12. Li X, Yang G, Fan M. Effects of homeobox gene distal-less 3 on proliferation and odontoblastic differentiation of human dental pulp cells. *J Endod* 2012; **38**: 1504–1510.

13. Hwang J, Mehrani T, Millar SE, Morasso MI. DLX3 is a crucial regulator of hair follicle differentiation and cycling. *Development* 2008; **135**: 3149–3159.
14. Choi SJ, Song IS, Ryu OH, Choi SW, Hart PS, Wu WW, Shen RF, Hart TC. A 4 bp deletion mutation in DLX3 enhances osteoblastic differentiation and bone formation in vitro. *Bone* 2008; **42**: 162–171.
15. Hassan MQ, Javed A, Morasso MI, Karlin J, Montecino M, van Wijnen AJ, Stein GS, Stein JL, Lian JB. Dlx3 transcriptional regulation of osteoblast differentiation: temporal recruitment of Msx2, Dlx3, and Dlx5 homeodomain proteins to chromatin of the osteocalcin gene. *Mol Cell Biol* 2004; **24**: 9248–9261.
16. Morasso MI, Markova NG, Sargent TD. Regulation of epidermal differentiation by a Distal-less homeodomain gene. *J Cell Biol* 1996; **135**: 1879–1887.
17. Pavlic A, Lukinmaa PL, Nieminen P, Kiukkonen A, Alaluusua S. Severely hypoplastic amelogenesis imperfecta with taurodontism. *Int J Paediatr Dent* 2007; **17**: 259–266.
18. Melnick M, Shields ED, El-Kafrawy AH. Tricho–dento–osseous syndrome: a scanning electron microscopic analysis. *Clin Genet* 1977; **12**: 17–27.
19. Jälevik B, Dietz W, Norén JG. Scanning electron micrograph analysis of hypomineralized enamel in permanent first molars. *Int J Paediatr Dent* 2005; **15**: 233–240.
20. Pavlic A, Petelin M, Battelino T. Phenotype and enamel ultrastructure characteristics in patients with ENAM gene mutations g.13185–13186insAG and 8344delG. *Arch Oral Biol* 2007; **53**: 209–217.
21. Wu XP, Liao EY, Zhang H, Dai RC, Shan PF, Cao XZ, Liu SP, Jiang YB. Determination of age-specific bone mineral density and comparison of diagnosis and prevalence of primary osteoporosis in Chinese women based on both Chinese and World Health Organization criteria. *J Bone Miner Metab* 2004; **22**: 382–391.
22. Kim JW, Simmer JP, Lin BP, Seymen F, Bartlett JD, Hu JC. Mutational analysis of candidate genes in 24 amelogenesis imperfecta families. *Eur J Oral Sci* 2006; **114**(Suppl. 1): 3–12.
23. Dong J, Amor D, Aldred MJ, Gu T, Escamilla M, MacDougall M. DLX3 mutation associated with autosomal dominant amelogenesis imperfecta with taurodontism. *Am J Med Genet A* 2005; **133**: 138–141.
24. Gorlin RJ, Cohen MM, Hennekam RCM. *Syndromes of the head and neck*, 4th revised edn. Oxford: Oxford University Press, 2001; 1232–1234.
25. Jälevik B, Odelius H, Dietz W, Norén J. Secondary ion mass spectrometry and X-ray microanalysis of hypomineralized enamel in human permanent first molars. *Arch Oral Biol* 2001; **46**: 239–247.
26. Seow WK. Taurodontism of the mandibular first permanent molar distinguishes between the tricho–dento–osseous (TDO) syndrome and amelogenesis imperfecta. *Clin Genet* 1993; **43**: 240–246.
27. Haldeman RJ, Cooper LF, Hart TC, Phillips C, Boyd C, Wright JT, Lester GE. Increased bone density associated with DLX3 mutation in the tricho–dento–osseous syndrome. *Bone* 2004; **35**: 988–997.
28. Jiang X, Iseki S, Maxson RE, Sucov HM, Morriss-Kay GM. Tissue origins and interactions in the mammalian skull vault. *Dev Biol* 2002; **241**: 106–116.
29. Chai Y, Maxson RE Jr. Recent advances in craniofacial morphogenesis. *Dev Dyn* 2006; **235**: 2353–2375.
30. Rodriguez-Leon J, Tomas AR, Johnson A, Kawakami Y. Recent advances in the study of limb development: the emergence and function of the apical ectodermal ridge. *J Stem Cells* 2013; **8**: 79–98.
31. Egawa S, Miura S, Yokoyama H, Endo T, Tamura K. Growth and differentiation of a long bone in limb development, repair and regeneration. *Dev Growth Differ* 2014; **56**: 410–424.
32. Selvaag E, Aas AM, Heide S. Structural hair shaft abnormalities in hypomelanosis of ito and other ectodermal dysplasia. *Acta Paediatr* 2000; **89**: 610–612.

Supporting Information

Additional Supporting Information may be found in the online version of this article:

Table S1. Clinical features of tricho–dento–osseous syndrome.

Fig. S1. DXA findings.

Fig. S2. Bioinformatical analysis of DLX3 Q178R mutation.